Instabilities of the *AA*-Stacked Graphene Bilayer

A. L. Rakhmanov,[1,2,3] A. V. Rozhkov,[1,2] A. O. Sboychakov,[1,2] and Franco Nori[1,4]

[1]*Advanced Science Institute, RIKEN, Wako-shi, Saitama, 351-0198, Japan*
[2]*Institute for Theoretical and Applied Electrodynamics, Russian Academy of Sciences, 125412 Moscow, Russia*
[3]*Moscow Institute for Physics and Technology (State University), 141700 Moscow Region, Russia*
[4]*Department of Physics, University of Michigan, Ann Arbor, Michigan 48109-1040, USA*
(Received 21 November 2011; published 13 November 2012)

Tight-binding calculations predict that the *AA*-stacked bilayer graphene has one electron and one hole conducting band, and that the Fermi surfaces of these bands coincide. We demonstrate that as a result of this degeneracy, the bilayer becomes unstable with respect to a set of spontaneous symmetry violations. Which of the symmetries is broken depends on the microscopic details of the system. For strong on-site Coulomb interaction we find that antiferromagnetism is the most stable order parameter. For an on-site repulsion energy typical for graphene systems, the antiferromagnetic gap can exist up to room temperature.

Introduction.—Graphene is a zero-gap semiconductor with a host of unusual electronic properties [1–3]. In recent years, bilayer graphene became a subject of numerous studies, partly driven by the desire to create graphene-based materials with an electronic gap. Moreover, bilayer graphene is an interesting material in its own right. Most efforts have focused on the study of the *AB*-stacked bilayer [4] for which high-quality samples are available [5,6]. Lately, the experimental realization of the *AA*-stacked graphene has been reported [7,8]. In this Letter, we discuss the electronic properties of *AA*-stacked bilayer graphene (*AA*-BLG), which, until recently, received very limited theoretical attention [8–12].

It is known that the *AA*-BLG tight-binding spectrum has four bands, of which one electron band and one hole band cross the Fermi energy [10]. The Fermi surfaces of these two bands coincide [9,10]. This feature has drastic consequences for the electronic properties of the bilayer because it enables several electron and electron-phonon instabilities, including: antiferromagnetism (AFM), current-ordered states, bilayer exciton condensation, and instability toward the shear shift of the layers. The type of ground state order depends on the microscopic details of the system and can be changed by applying stress, external pressure, the presence or absence of the substrate, etc. Below we will limit our attention to the AFM order and the structural instability with respect to the shear layer shift (shear instability for short). These two choices are justified. The on-site Coulomb repulsion is the strongest interaction in the *AA*-BLG system, and this interaction is sufficient to guarantee the stability or metastability of the AFM order. As for the shear instability, there are experimental [13,14] and numerical [15] suggestions that *AA*-stacked graphene multilayers may be unstable with respect to the mechanical displacement of the layers with respect to each other. However, our calculations show that the shear instability

driven by the conducting electrons seems to have a crossover temperature which is too low to be experimentally observable.

The model.—In the *AA*-BLG, carbon atoms of the upper layer are located on top of the equivalent atoms of the bottom layer. The system is modeled by the tight-binding Hamiltonian for p_z electrons of carbon atoms

$$H_0 = -t \sum_{\langle \mathbf{nm} \rangle i\sigma} a^\dagger_{\mathbf{n}i\sigma} b_{\mathbf{m}i\sigma} - t_0 \sum_{\mathbf{n}\sigma} a^\dagger_{\mathbf{n}1\sigma} a_{\mathbf{n}2\sigma} - t_0 \sum_{\mathbf{m}\sigma} b^\dagger_{\mathbf{m}1\sigma} b_{\mathbf{m}2\sigma}$$
$$- t_g \sum_{\langle \mathbf{nm} \rangle \sigma} (a^\dagger_{\mathbf{n}1\sigma} b_{\mathbf{m}2\sigma} + a^\dagger_{\mathbf{n}2\sigma} b_{\mathbf{m}1\sigma}) + \text{H.c.} \quad (1)$$

Here $a^\dagger_{\mathbf{n}i\sigma}$ and $a_{\mathbf{n}i\sigma}$ ($b^\dagger_{\mathbf{m}i\sigma}$ and $b_{\mathbf{m}i\sigma}$) are creation and annihilation operators of an electron with spin σ in the layer $i = 1$, 2 on the sublattice $\mathcal{A}$ ($\mathcal{B}$) at site $\mathbf{n} \in \mathcal{A}$ ($\mathbf{m} \in \mathcal{B}$). The amplitude t (t_0) in Eq. (1) describes the in-plane (interplane) nearest-neighbor hopping, while t_g corresponds to the interlayer next-nearest neighbor hopping. The interplane distance in bilayer graphene $c \approx$ 3.3 Å [8], and it is larger than the in-plane carbon-carbon distance $a \approx 1.4$ Å. Thus, the in-plane hopping integral t is larger than the interplane one, t_0. For calculations we will use the characteristic values $t \approx 2.57$ eV, $t_0 \approx$ 0.36 eV, $t_g \approx -0.03$ eV [16]. We omit next-next-nearest neighbor hopping between $\mathcal{A}$ ($\mathcal{B}$) sites since the corresponding term only shifts the zero-energy level.

The elementary unit cell of bilayer graphene consists of four atoms. It is convenient to introduce the bispinors $\psi^\dagger_{\mathbf{k}\sigma} = (\psi^\dagger_{\mathbf{k}\mathcal{A}\sigma}, \psi^\dagger_{\mathbf{k}\mathcal{B}\sigma})$, with spinor components $\psi^\dagger_{\mathbf{k}\mathcal{A}\sigma} = (a^\dagger_{\mathbf{k}1\sigma}, a^\dagger_{\mathbf{k}2\sigma})$ and $\psi^\dagger_{\mathbf{k}\mathcal{B}\sigma} = e^{-i\varphi_{\mathbf{k}}}(b^\dagger_{\mathbf{k}1\sigma}, b^\dagger_{\mathbf{k}2\sigma})$, where $\varphi_{\mathbf{k}} = \arg\{f_{\mathbf{k}}\}$, and

$$f_{\mathbf{k}} = 1 + 2\exp\left(\frac{3ik_x a}{2}\right)\cos\left(\frac{k_y a\sqrt{3}}{2}\right). \quad (2)$$

The components of the spinors $\psi^\dagger_{\mathbf{k}\mathcal{A}\sigma}$, $\psi^\dagger_{\mathbf{k}\mathcal{B}\sigma}$ have different values of the layer index.

Let us define a set of Pauli matrices $\hat{\tau}_\alpha$ acting on the layer index, and a second set $\hat{\sigma}_\alpha$ of Pauli matrices acting on the sublattice index. In terms of these matrices, the bilayer Hamiltonian in **k**-space can be written as $\hat{H}_{0\mathbf{k}} = -[t_0\hat{\tau}_x + (t + t_g\hat{\tau}_x)\hat{\sigma}_x|f_\mathbf{k}|]$, or, explicitly

$$\hat{H}_{0\mathbf{k}} = -\begin{pmatrix} 0 & t_0 & t|f_\mathbf{k}| & t_g|f_\mathbf{k}| \\ t_0 & 0 & t_g|f_\mathbf{k}| & t|f_\mathbf{k}| \\ t|f_\mathbf{k}| & t_g|f_\mathbf{k}| & 0 & t_0 \\ t_g|f_\mathbf{k}| & t|f_\mathbf{k}| & t_0 & 0 \end{pmatrix}. \quad (3)$$

The phase shift $e^{-i\varphi_\mathbf{k}}$ introduced in the definition of the spinors $\psi^\dagger_{\mathbf{k}\mathcal{B}\sigma}$ makes $\hat{H}_{0\mathbf{k}}$ real. The Hamiltonian (3) is invariant under the transposition of the sublattices and of the graphene layers. That is, $[\hat{\sigma}_x, \hat{H}_{0\mathbf{k}}] = [\hat{\tau}_x, \hat{H}_{0\mathbf{k}}] = 0$. Thus, the eigenvectors of the matrix (3) can be classified according to the quantum numbers σ and τ, which characterize the eigenvector parity under σ_x and τ_x transformations. Using these symmetries it is easy to find the transformation $\hat{U}$ which diagonalizes $\hat{H}_{0\mathbf{k}}$:

$$\hat{U} = \frac{1}{2}(\hat{\tau}_x + \hat{\tau}_z)(\hat{\sigma}_x + \hat{\sigma}_z) = \hat{U}^{-1}. \quad (4)$$

The electron spectrum $\varepsilon^{(s)}_\mathbf{k}$ consists of four bands, and each band has a unique value of the pair (σ, τ):

$$\varepsilon^{(1)}_\mathbf{k} = -t_0 - (t + t_g)|f_\mathbf{k}|, \qquad \sigma = 1, \qquad \tau = 1, \quad (5)$$

$$\varepsilon^{(2)}_\mathbf{k} = +t_0 - (t - t_g)|f_\mathbf{k}|, \qquad \sigma = 1, \qquad \tau = -1, \quad (6)$$

$$\varepsilon^{(3)}_\mathbf{k} = -t_0 + (t + t_g)|f_\mathbf{k}|, \qquad \sigma = -1, \qquad \tau = 1, \quad (7)$$

$$\varepsilon^{(4)}_\mathbf{k} = +t_0 + (t - t_g)|f_\mathbf{k}|, \qquad \sigma = -1, \qquad \tau = -1. \quad (8)$$

The band structure is shown in Fig. 1. The bands $s = 2$ and $s = 3$ cross the Fermi energy level near the Dirac point $\mathcal{K}$, located at momentum $\mathbf{K} = 2\pi\{\sqrt{3}, 1\}/(3\sqrt{3}a)$ and the Dirac point $\mathcal{K}'$ located at momentum $\mathbf{K}' = 2\pi\{\sqrt{3}, -1\}/(3\sqrt{3}a)$ [see Fig. 1(b)]. The most interesting feature of this band structure is that at half-filling (which corresponds to undoped AA-BLG) the Fermi surfaces of both bands coincide. The Fermi level is $\varepsilon_\mathrm{F} = t_g t_0/t \approx -0.004$ eV, while the Fermi surfaces are given by the equation $|f_\mathbf{k}| = t_0/t$. For $t_0/t \ll 1$, one can expand the function $|f_\mathbf{k}|$ near the Dirac points and demonstrate that the Fermi surface consists of six arcs inside the first Brillouin zone with the radius $k_r = 2t_0/(3ta)$ [Fig. 1(c)].

The matching of the Fermi surfaces is quite stable against changes in the tight-binding Hamiltonian. First, it survives if we add more distant hopping terms to H_0. Moreover, even layer-asymmetric systems (e.g., similar to the single-side hydrogenated graphene [17]) possess this property. However, it is clear that the different types of
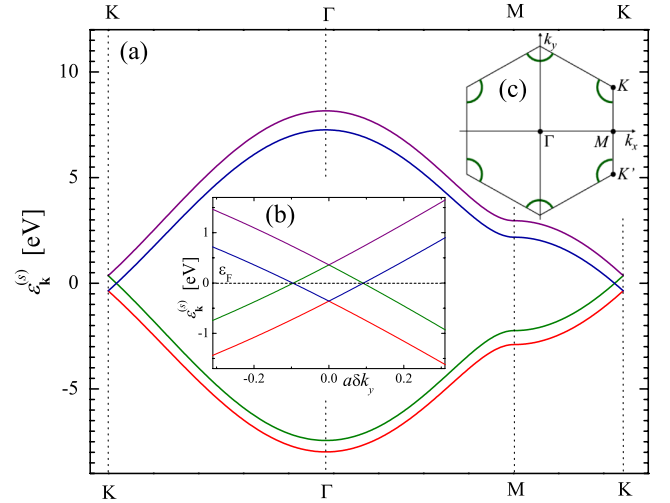

FIG. 1 (color online).   (a) The band structure of the AA-stacked bilayer graphene. (b) The **k**-dependence of the spectra $\varepsilon^{(s)}_\mathbf{k}$ near the Dirac point $\mathcal{K}$ located at momentum $\mathbf{K}$; $\mathbf{k} = \mathbf{K} + \delta k_y\mathbf{e}_y$. Bands $s = 2$ and $s = 3$ intersect at the Fermi level ($\varepsilon_\mathrm{F} \approx -0.004$ eV). (c) Solid (green) arcs show six fragments of the Fermi surface in the first Brillouin zone.

interactions (e.g., electron-electron, electron-phonon) can destabilize such a degenerate spectrum.

Mean-field Hamiltonian.—The presence of two bands with identical Fermi surfaces makes the system unstable with respect to spontaneous symmetry breaking. We will demonstrate that the Hamiltonian symmetries σ_x and τ_x can be used to narrow the possible symmetry choices.

In a mean-field approach, the two-particle interaction operator $H_\mathrm{int} \propto \psi^\dagger \psi^\dagger \psi \psi$ is replaced by a single-particle operator $\delta H_\mathrm{int} \propto \langle\psi^\dagger\psi\rangle\psi^\dagger\psi$, where the average $\langle\psi^\dagger\psi\rangle$ represents different types of nonsuperconducting order parameters. The values of these order parameters are found from the self-consistency conditions. To be at least metastable, the order parameter must open a gap at the Fermi level. The most general form of δH_int, which can open an insulating gap, is

$$\delta H_\mathrm{int} = \sum_{\mathbf{k}\sigma} \psi^\dagger_{\mathbf{k}\sigma} \delta\hat{H}_{\mathbf{k}\sigma} \psi_{\mathbf{k}\sigma},$$

$$\delta\hat{H}_{\mathbf{k}\sigma} = \sum_\alpha (\Delta^\alpha_{\mathcal{AB}\mathbf{k}\sigma}\hat{\sigma}_\alpha + \Delta^\alpha_{12\mathbf{k}\sigma}\hat{\tau}_\alpha) + \sum_{\alpha\beta}\Delta^{\alpha\beta}_{\mathbf{k}\sigma}\hat{\tau}_\alpha\hat{\sigma}_\beta, \quad (9)$$

where $\Delta^\alpha_{\mathcal{AB}\mathbf{k}\sigma}$, $\Delta^\alpha_{12\mathbf{k}\sigma}$, and $\Delta^{\alpha\beta}_{\mathbf{k}\sigma}$ are real-valued order parameters, which, in general, are functions of **k**. To open a gap, the corresponding term in δH_int must couple the conducting bands $\varepsilon^{(2)}_\mathbf{k}$ and $\varepsilon^{(3)}_\mathbf{k}$. Observe that these bands have unequal values of σ and τ [see Eqs. (6) and (7)]. Therefore, $\Delta^{\alpha\beta}_{\mathbf{k}\sigma}$ couples the bands and opens the gap only when α, $\beta \neq x$. Otherwise, $\Delta^{\alpha\beta}_{\mathbf{k}\sigma}$ commutes either with σ_x or τ_x, and, consequently, do not open the gap.

To calculate the renormalized bands near the Fermi level, we should diagonalize the matrix $\hat{H}_{\mathbf{k}\sigma} = \hat{H}_{0\mathbf{k}} + \delta\hat{H}_{\mathbf{k}\sigma}$. Transforming $\hat{H}_{\mathbf{k}\sigma}$ with the $\hat{U}$ given by Eq. (4), we find

$$\hat{U}^{-1}\hat{H}_{\mathbf{k}\sigma}\hat{U} = \begin{pmatrix} \ddots & \cdots & \cdots & \cdots \\ \vdots & \varepsilon_{\mathbf{k}}^{(2)} + \delta\varepsilon_{\mathbf{k}\sigma}^{(2)} & \Delta_{\mathbf{k}\sigma} & \vdots \\ \vdots & \Delta_{\mathbf{k}\sigma}^{*} & \varepsilon_{\mathbf{k}}^{(3)} + \delta\varepsilon_{\mathbf{k}\sigma}^{(3)} & \vdots \\ \cdots & \cdots & \cdots & \ddots \end{pmatrix},$$

(10)

where $\delta\varepsilon_{\mathbf{k}\sigma}^{(2)} = \Delta_{\mathcal{AB}\mathbf{k}\sigma}^{x} - \Delta_{12\mathbf{k}\sigma}^{x} - \Delta_{\mathbf{k}\sigma}^{xx}$, $\delta\varepsilon_{\mathbf{k}\sigma}^{(3)} = -\Delta_{\mathcal{AB}\mathbf{k}\sigma}^{x} + \Delta_{12\mathbf{k}\sigma}^{x} - \Delta_{\mathbf{k}\sigma}^{xx}$, and $\Delta_{\mathbf{k}\sigma} = \Delta_{\mathbf{k}\sigma}^{zz} + \Delta_{\mathbf{k}\sigma}^{yy} + i(\Delta_{\mathbf{k}\sigma}^{zy} + \Delta_{\mathbf{k}\sigma}^{yz})$. Other elements of this matrix are unimportant for further consideration. Solving the secular equation for the 2×2 matrix in Eq. (10), we obtain the renormalized spectrum of the bands with $s = 2, 3$:

$$E_{\mathbf{k}\sigma}^{(2,3)} = \frac{1}{2}(\varepsilon_{\mathbf{k}}^{(2)} + \delta\varepsilon_{\mathbf{k}\sigma}^{(2)} + \varepsilon_{\mathbf{k}}^{(3)} + \delta\varepsilon_{\mathbf{k}\sigma}^{(3)})$$
$$\mp \frac{1}{2}\sqrt{(\varepsilon_{\mathbf{k}}^{(2)} + \delta\varepsilon_{\mathbf{k}\sigma}^{(2)} - \varepsilon_{\mathbf{k}}^{(3)} - \delta\varepsilon_{\mathbf{k}\sigma}^{(3)})^2 + 4|\Delta_{\mathbf{k}\sigma}|^2}.$$ (11)

The gap between renormalized bands is equal to $\Delta_0 = 2\min_{\mathbf{k}}|\Delta_{\mathbf{k}\sigma}|$. We see that the contribution to the gap comes only from the $\Delta_{\mathbf{k}\sigma}^{zz}$, $\Delta_{\mathbf{k}\sigma}^{yy}$, $\Delta_{\mathbf{k}\sigma}^{zy}$, and $\Delta_{\mathbf{k}\sigma}^{yz}$ order parameters, which break down both sublattice and layer symmetries. It is easy to show that other elements of the full 4×4 matrix (10) give only a second-order contribution to this result. Neglecting other order parameters, the matrix $\delta\hat{H}_{\mathbf{k}\sigma}$ can be written in the form

$$\delta\hat{H}_{\mathbf{k}\sigma} = \begin{pmatrix} \Delta_{\mathbf{k}\sigma}^{zz} & -i\Delta_{\mathbf{k}\sigma}^{yz} & -i\Delta_{\mathbf{k}\sigma}^{zy} & -\Delta_{\mathbf{k}\sigma}^{yy} \\ i\Delta_{\mathbf{k}\sigma}^{yz} & -\Delta_{\mathbf{k}\sigma}^{zz} & \Delta_{\mathbf{k}\sigma}^{yy} & i\Delta_{\mathbf{k}\sigma}^{zy} \\ i\Delta_{\mathbf{k}\sigma}^{zy} & \Delta_{\mathbf{k}\sigma}^{yy} & -\Delta_{\mathbf{k}\sigma}^{zz} & i\Delta_{\mathbf{k}\sigma}^{yz} \\ -\Delta_{\mathbf{k}\sigma}^{yy} & -i\Delta_{\mathbf{k}\sigma}^{zy} & -i\Delta_{\mathbf{k}\sigma}^{yz} & \Delta_{\mathbf{k}\sigma}^{zz} \end{pmatrix}.$$ (12)

Here, all gap-inducing order parameters allowed by the symmetry are included. To obtain the ground state, we have to calculate the system energy and minimize it by varying the Δ's. However, this procedure is prohibitively complex mathematically. In practice, we specify a particular interaction and the types of order parameters consistent with it. Then we calculate the system energy for each order parameter. The parameter with the lowest energy corresponds to the ground state. Below we will show that $\Delta_{\mathbf{k}\sigma}^{zz}$ can be related to the G-type antiferromagnetic order parameter (i.e., each spin is antiparallel to all its nearest-neighboring spins) produced by the on-site Coulomb repulsion. The $\Delta_{\mathbf{k}\sigma}^{yy}$ can be attributed to the instability toward the homogeneous shift of one graphene layer with respect to another. The order parameters $\Delta_{\mathbf{k}\sigma}^{zy}$ and $\Delta_{\mathbf{k}\sigma}^{yz}$ can correspond, e.g., to excitons, which produce a current flowing inside and between the layers, respectively.

Antiferromagnetic state.—It is known that the Coulomb interaction among electrons in graphene is rather strong and the value of the on-site Coulomb repulsion energy $U \sim 10$ eV [18]. However, graphene remains semimetal since

the electron density of states at the Fermi level is zero. In contrast, the AA-BLG has a Fermi surface, and the density of states at the Fermi level is finite. Then, one can expect that the role of electron-electron interactions in AA-BLG is more important and it can affect the ground state. Here we only consider the on-site Coulomb interaction. We write the Hubbard Hamiltonian

$$H_{\text{int}} = \frac{U}{2}\sum_{\mathbf{n}i\sigma}n_{\mathbf{n}i\mathcal{A}\sigma}n_{\mathbf{n}i\mathcal{A}\bar{\sigma}} + \frac{U}{2}\sum_{\mathbf{m}i\sigma}n_{\mathbf{m}i\mathcal{B}\sigma}n_{\mathbf{m}i\mathcal{B}\bar{\sigma}},$$ (13)

where $n_{\mathbf{n}i\mathcal{A}\sigma} = a_{\mathbf{n}i\sigma}^{\dagger}a_{\mathbf{n}i\sigma}$, $n_{\mathbf{m}i\mathcal{B}\sigma} = b_{\mathbf{m}i\sigma}^{\dagger}b_{\mathbf{m}i\sigma}$, and $\bar{\sigma} = -\sigma$. It is known that the ground state of Hubbard-like models at half-filling can be antiferromagnetic. For the AA-BLG symmetry, three types of AFM ordering (having different spin arrangement inside the unit cell) are possible. However, only the G-type AFM order opens a gap at the Fermi level even if the interaction is arbitrarily small. Two other types of AFM order do not break down both sublattice and layer symmetries and, therefore, they do not open a gap at the Fermi level. Consequently, they are unstable for small U (and metastable for large U).

In mean-field, $n_{\mathbf{n}ia\sigma}$ ($a = \mathcal{A}, \mathcal{B}$) in Eq. (13) has the form $n_{\mathbf{n}ia\sigma} = n_{ia\sigma} + \delta n_{\mathbf{n}ia\sigma}$, where $n_{ia\sigma} = \langle n_{\mathbf{n}ia\sigma}\rangle$ and $\delta n_{\mathbf{n}ia\sigma} = n_{\mathbf{n}ia\sigma} - n_{ia\sigma}$. The mean-field Hamiltonian is obtained then by neglecting the terms quadratic in $\delta n_{\mathbf{n}ia\sigma}$. For G-type AFM, the spin-up and spin-down electron densities are redistributed as $n_{1\mathcal{A}\uparrow} = n_{2\mathcal{B}\uparrow} = n_{2\mathcal{A}\downarrow} = n_{1\mathcal{B}\downarrow} = (1 + \Delta n)/2$, and $n_{1\mathcal{A}\downarrow} = n_{2\mathcal{B}\downarrow} = n_{2\mathcal{A}\uparrow} = n_{1\mathcal{B}\uparrow} = (1 - \Delta n)/2$, while the total on-site electron density $n_{ia\sigma} + n_{ia\bar{\sigma}}$ remains equal to unity. Thus, the mean-field interaction Hamiltonian has the form of Eq. (9) with $\Delta_{\mathbf{k}\uparrow}^{zz} = -\Delta$, $\Delta_{\mathbf{k}\downarrow}^{zz} = +\Delta$, and $\Delta = U\Delta n/2$. Other terms in Eq. (9) are equal to zero.

The eigenvalues $E_{\mathbf{k}\sigma}^{(s)}$ and eigenvectors $v_{p\mathbf{k}\sigma}^{(s)}$ of the matrices $\hat{H}_{\mathbf{k}\sigma} = \hat{H}_{0\mathbf{k}} + \delta\hat{H}_{\mathbf{k}\sigma}$ can be found analytically. The spectra of spin-up and spin-down electrons are equal. The bands 2 and 3 are given by Eq. (11) with $\delta\varepsilon_{\mathbf{k}\sigma}^{(2)} = \delta\varepsilon_{\mathbf{k}\sigma}^{(3)} = 0$, and $|\Delta_{\mathbf{k}\sigma}| = \Delta$. The bands 1 and 4 are given by Eq. (11) where $\varepsilon_{\mathbf{k}}^{(2,3)}$ is replaced by $\varepsilon_{\mathbf{k}}^{(1,4)}$. When the gap is open, the lower two bands are filled, while the upper two are empty. To find the value of the gap, one needs to solve the self-consistent equation for $\Delta n = 2\Delta/U$:

$$n_{1\mathcal{A}\uparrow} = \frac{1}{2} + \frac{\Delta}{U} = \sum_{s=1,2}\int\frac{d\mathbf{k}}{V_{\text{BZ}}}|v_{1\mathbf{k}\uparrow}^{(s)}|^2$$
$$= \frac{1}{2} + \frac{1}{4}\int\frac{d\mathbf{k}}{V_{\text{BZ}}}\left[\frac{\Delta}{\sqrt{\Delta^2 + (t|f_{\mathbf{k}}| + t_0)^2}}\right.$$
$$\left.+ \frac{\Delta}{\sqrt{\Delta^2 + (t|f_{\mathbf{k}}| - t_0)^2}}\right],$$ (14)

where $V_{\text{BZ}} = 8\pi^2/(3\sqrt{3}a^2)$ is the area of the first Brillouin zone. We introduce the dimensionless density of states

$\rho_0(\zeta) = \int d\mathbf{k}\,\delta(\zeta - |f_\mathbf{k}|)/V_{BZ}$ [$\rho_0(\zeta) \neq 0$ for $0 < \zeta < 3$], which is related [1] to the graphene density of states $\rho_{gr}(E)$ according to $\rho_{gr}(E) = \rho_0(|E/t|)/t$. Equation (14) then becomes

$$\int_0^3 d\zeta \left[\frac{\rho_0(\zeta)}{\sqrt{\delta^2 + (\zeta + \zeta_0)^2}} + \frac{\rho_0(\zeta)}{\sqrt{\delta^2 + (\zeta - \zeta_0)^2}} \right] = \frac{4t}{U}, \quad (15)$$

where $\delta = \Delta/t$ and $\zeta_0 = t_0/t$. The integral of the second term in the left-hand side of Eq. (15) diverges logarithmically when $\Delta \to 0$. In the limit of small Δ, from Eq. (15) one can derive

$$\Delta = 2\sqrt{t_0(3t - t_0)} \exp\left\{ -\frac{4t - U\eta(\zeta_0)}{2U\rho_0(\zeta_0)} \right\}, \quad (16)$$

where

$$\eta(\zeta_0) = \int_0^3 d\zeta \left[\frac{\rho_0(\zeta)}{\zeta + \zeta_0} + \frac{\rho_0(\zeta) - \rho_0(\zeta_0)}{|\zeta - \zeta_0|} \right]. \quad (17)$$

Figure 2 shows the dependence of Δ on U. Taking the value of $U = 8$ or 9 eV [18], we obtain $\Delta \cong 2$ or 3 eV and the magnetic moment at each site $\mu_B \Delta n$ is about 1 μ_B. However, the exact value of U for AA-BLG is not known.

Discussion.—The calculations above were done at $T = 0$. For $T > 0$, the long-range AFM order is destroyed by spin-wave fluctuations. The latter may be described using the nonlinear σ-model with Lagrangian [19,20]
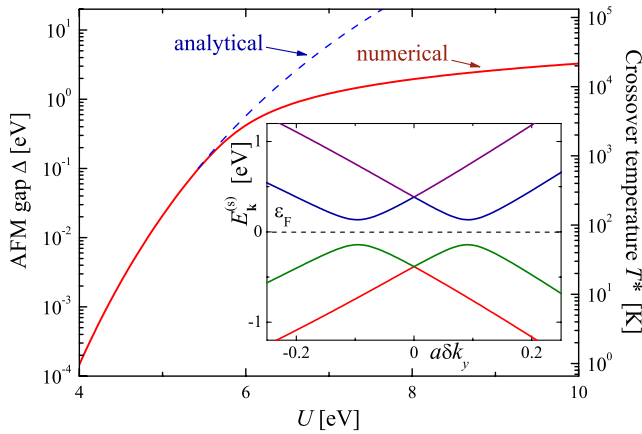

FIG. 2 (color online). AFM gap Δ at $T = 0$ (left y axis) and crossover temperature T^* (right y axis) versus the on-site Coulomb repulsion U. The solid (red) curve is calculated by solving Eq. (15), while the dashed (blue) curve is calculated from Eq. (16). The crossover temperature T^* is proportional to Δ. The figure can be considered as a phase diagram in the U-T plane, where the solid (red) curve separates the AFM short-range order phase from the paramagnetic metallic phase. The inset shows the electron spectrum near the $\mathcal{K}$ point at $U = 5.5$ eV ($\Delta \approx 0.12$ eV).

$$\mathcal{L}_{sw} = \frac{\rho}{2}[(\partial_t \mathbf{n})^2 + c_{sw}^2(\partial_\mathbf{r} \mathbf{n})^2], \qquad |\mathbf{n}| = 1, \quad (18)$$

where the unit vector $\mathbf{n}$ is the direction of the AFM ordering. The spin-wave stiffness ρ and their velocity c_{sw} can be evaluated from Eqs. (7.89), (7.90) of Ref. [21]:

$$c_{sw} = \frac{3at}{2\sqrt{2}} = \frac{v_F}{\sqrt{2}}, \qquad \rho = \begin{cases} t_0/(8\pi v_F^2), & \text{if } t_0 \gg \Delta, \\ \Delta/(16\pi v_F^2), & \text{if } t_0 \ll \Delta. \end{cases} \quad (19)$$

After standard calculations [19,20] we obtain the spin-wave correlation length $\xi_{sw} \sim (c_{sw}/T) \exp(2\pi\rho c_{sw}^2/T)$, describing the characteristic size of the short-range AFM order. This expression is valid until ξ_{sw} is larger than the mean-field correlation length $\xi \sim v_F/\Delta(T)$; otherwise, Eq. (18) is inapplicable, and no short-range order exists. The condition $\xi_{sw} = \xi$ defines the crossover temperature T^* between the short-range AFM and the paramagnet. Simple analysis gives $T^* \sim \Delta$ for all values of t_0 and Δ. Below T^* the short-range AFM order exists on distances about $\xi_{sw} \gg a$, and this order is destroyed if $T > T^*$. We plot T^* versus U in Fig. 2

Imperfections of the sample, effects of the substrate, etc., can also affect the AFM order. However, if the energy disturbance produced by these factors is smaller than Δ, they only amount to perturbative corrections.

Other possible types of ordering could be considered following the same approach used for AFM. However, whether a particular order is stable and observable depends on the values of the hopping amplitudes and a characteristic energy of the appropriate interaction. For example, applying the mean field approximation to the model with on-site repulsion we find that the charge density wave is unstable for our choice of parameters.

The next evident possibility to open a gap is to shear one graphene layer with respect to another. For illustration, we consider a shift along the C-C bond. The shift u deforms the shape of the unit cell, changing $\mathcal{A}\mathcal{B}$ bonds between different layers, and giving rise to the appearance of the order parameter $\Delta_{\mathbf{k}\sigma}^{yy}$. Assuming that the hopping amplitude t_g changes linearly with u, we can write for different bonds $t_g(u) \approx t_g(0) \pm (\partial t_g/\partial u)u$. Now the electronic energy of the system becomes a function of u. Taking into account the elastic contribution $C_{sh}u^2/2$ (where C_{sh} is the shear modulus) to the total energy and minimizing this energy with respect to u, we obtain the value of the equilibrium shift between the layers

$$u_{eq} \approx \frac{t}{|\partial t_g/\partial u|} \exp\left[-\frac{\pi C_{sh}a^2t^2}{(\partial t_g/\partial u)^2 ct_0} \right]. \quad (20)$$

If we assume that C_{sh} is about the shear modulus in graphite and $|\partial t_g/\partial u| \sim t_g/a$, we conclude that the shift u_{eq} and the corresponding energy gain are too small to be observable. However, this conclusion must be taken cautiously. First, we have no accurate information on C_{sh} and $|\partial t_g/\partial u|$, whose precise values are important for the

estimate of u_{eq}. Moreover, u_{eq} could be enhanced by pressure or the presence of a substrate. Finally, the shift can be induced by a different mechanism.

Compared to AA stacking, graphene bilayers with AB stacking have a different electronic structure and symmetries of the Hamiltonian. Thus, the magnetic and electronic properties of the AA and AB-BLG should be different even for the same values of the hopping integrals and on-site Coulomb repulsion U.

In conclusion, we demonstrate that the AA-BLG is unstable with respect to a set of symmetry-breaking instabilities, which can give rise to several order parameters of different nature (e.g., magnetic, mechanical, current-carrying). We show that an AFM order can be observed in the system. The possible existence of other types of orders in the AA-BLG depends on the system parameters and the external conditions (temperature, pressure, substrate, etc.).

[1] A. H. Castro Neto, F. Guinea, N. M. R. Peres, K. S. Novoselov, and A. K. Geim, Rev. Mod. Phys. **81,** 109 (2009).

[2] D. S. L. Abergel, V. Apalkov, J. Berashevich, K. Ziegler, and T. Chakraborty, Adv. Phys. **59,** 261 (2010).

[3] A. Rozhkov, G. Giavaras, Y. P. Bliokh, V. Freilikher, and F. Nori, Phys. Rep. **503,** 77 (2011).

[4] E. McCann and V. I. Fal'ko, Phys. Rev. Lett. **96,** 086805 (2006); E. V. Castro, N. M. R. Peres, T. Stauber, and N. A. P. Silva, ibid. **100,** 186803 (2008); R. Nandkishore and L. Levitov, ibid. **104,** 156803 (2010); Phys. Rev. B **82,** 115124 (2010); F. Zhang, H. Min, M. Polini, and A. H. MacDonald, ibid. **81,** 041402 (2010); Y. Lemonik, I. L. Aleiner, C. Toke, and V. I. Fal'ko, ibid. **82,** 201408 (2010);

[5] B. E. Feldman, J. Martin, and A. Yacoby, Nat. Phys. **5,** 889 (2009).

[6] A. S. Mayorov, D. C. Elias, M. Mucha-Kruczynski, R. V. Gorbachev, T. Tudorovskiy, A. Zhukov, S. V. Morozov, M. I. Katsnelson, V. I. Fal'ko, A. K. Geim, and K. S. Novoselov, Science **333,** 860 (2011).

[7] Z. Liu, K. Suenaga, P. J. F. Harris, and S. Iijima, Phys. Rev. Lett. **102,** 015501 (2009).

[8] J. Borysiuk, J. Soltys, and J. Piechota, J. Appl. Phys. **109,** 093523 (2011).

[9] P. L. de Andres, R. Ramírez, and J. A. Vergés, Phys. Rev. B **77,** 045403 (2008).

[10] E. Prada, P. San-Jose, L. Brey, and H. Fertig, Solid State Commun. **151,** 1075 (2011).

[11] C. W. Chiu, S. H. Lee, S. C. Chen, F. L. Shyu, and M. F. Lin, New J. Phys. **12,** 083060 (2010).

[12] Y.-H. Ho, J.-Y. Wu, R.-B. Chen, Y.-H. Chiu, and M.-F. Lin, Appl. Phys. Lett. **97,** 101905 (2010).

[13] J. Hass, F. Varchon, J. E. Millán-Otoya, M. Sprinkle, N. Sharma, W. A. de Heer, C. Berger, P. N. First, L. Magaud, and E. H. Conrad, Phys. Rev. Lett. **100,** 125504 (2008).

[14] F. Varchon, P. Mallet, L. Magaud, and J.-Y. Veuillen, Phys. Rev. B **77,** 165415 (2008).

[15] J. Berashevich and T. Chakraborty, Phys. Rev. B **84,** 033403 (2011).

[16] J.-C. Charlier, J.-P. Michenaud, and X. Gonze, Phys. Rev. B **46,** 4531 (1992).

[17] H. J. Xiang, E. J. Kan, S. H. Wei, X. G. Gong, and M. H. Whangbo, Phys. Rev. B **82,** 165425 (2010); B. S. Pujari, S. Gusarov, M. Brett, and A. Kovalenko, Phys. Rev. B **84,** 041402(R) (2011); L. Openov and A. Podlivaev, Semiconductors **46,** 199 (2012).

[18] T. O. Wehling, E. Şaşıoğlu, C. Friedrich, A. I. Lichtenstein, M. I. Katsnelson, and S. Blügel, Phys. Rev. Lett. **106,** 236805 (2011).

[19] S. Chakravarty, B. I. Halperin, and D. R. Nelson, Phys. Rev. B **39,** 2344 (1989).

[20] E. Manousakis, Rev. Mod. Phys. **63,** 1 (1991).

[21] A. M. J. Schakel, *Boulevard of Broken Symmetries: Effective Field Theories of Condensed Matter* (World Scientific, Singapore, 2008).